Simulation of the intermolecular vibrational spectra of liquid water and water clusters

Wayne B. Bosma,[a] Laurence E. Fried,[b] and Shaul Mukamel
Department of Chemistry, University of Rochester, Rochester, New York 14627

(Received 26 October 1992; accepted 10 December 1992)

We report simulated Raman and infrared spectra of liquid water and water clusters in the frequency range 0–1000 cm^{-1}. The librational peak in the Raman spectrum of the liquid, which has a strong dependence on the anisotropy of the assumed gas-phase polarizability tensor, allows us to choose between various models for that tensor. Most of the spectroscopically probed dynamics of the liquid are present in the small clusters, with N as low as 5. The librational peaks in the pentamer spectra are shown to redshift with increasing temperature.

I. INTRODUCTION

Water is among the most studied of chemicals, owing, in part, to its ubiquity and its necessity for all life. In addition to these "natural" reasons, water is an interesting compound because it has unique physical properties and is a model hydrogen-bonded liquid. Computer simulations of liquid water have been performed for more than two decades now, since the pioneering work of Rahman and Stillinger in 1971.[1] Since then, simulations have provided a great deal of insight into the physical properties of water; however, there are still very fundamental open questions regarding the microscopic dynamics of the individual molecules in the liquid. These questions are crucial for the interpretation of the intermolecular Raman (or Rayleigh-wing) spectrum of the liquid, which extends from 0 to 1000 cm^{-1}.

The intermolecular Raman spectrum of liquid water is rich with information,[2–7] having, in addition to the zero-frequency (Rayleigh) component, a well-defined peak near 170 cm^{-1}, as well as a faint peak near 60 cm^{-1} and a very broad "tail" extending from around 300 to 1000 cm^{-1}. The features in the 0–300 cm^{-1} region have been reproduced by molecular dynamics simulations using pairwise additive potentials and rigid molecules.[8,9] Madden and co-workers[8] have simulated the Raman spectrum using the Matsuoka–Clementi–Yoshimine (MCY) potential,[10] and Ricci, Ruocco, and Sampoli[9] have generated similar results using the transferrable intermolecular potential (TIP4P) model.[11] The origins of the low-frequency Raman peaks are believed to be as follows:[3] The 60 cm^{-1} peak results from the bending of the hydrogen bonds between water molecules, the 170 cm^{-1} peak is due to the stretching of hydrogen bonds, and the structure in the 300–1000 cm^{-1} region is due to molecular librations. Some studies, however, attribute the two lower-frequency features to the dipole moments induced by the dipoles on the surrounding molecules,[8,9(a)] and assert that the hydrogen bonding which occurs in water is not necessary to describe the low-frequency Raman spectrum. Some recent experiments[5] have used isotope substitution, and attribute the 170 cm^{-1} peak to primarily oxygen–oxygen motion. Other recent experimental[6] and theoretical[12] works ascribe the motions underlying the intermolecular vibrations to more collective motions, involving at least a few tens of molecules.

The far-infrared (IR) spectrum of water contains vibrational information which is complementary to the low-frequency Raman spectrum, due to the different selection rules of the two spectroscopies. The low-frequency IR spectrum is dominated by a peak in the librational region; the 170 and 60 cm^{-1} peaks are much less pronounced. The IR spectrum of liquid water has been calculated using rigid-molecule molecular dynamics,[8,13] one recent study,[13] using the simple point charge (SPC) model[14] for water, produced results which compared well to experimental results from 1–1000 cm^{-1}. Reference 13 summarizes the current state of using molecular dynamics (MD) to simulate the vibrational spectroscopy of water. The agreement of simulation and experiment was quantitative (including the absolute magnitude). This should not be taken for granted, as the relevant dynamics are characterized by frequencies which are high compared to k_BT (k_B is Boltzmann's constant and T is temperature), where quantum effects could be significant.

In attempting to determine the dynamics underlying the Raman and IR spectra of water, it is natural to try to think of a typical molecule and its local environment. If, by studying just a few molecules, we may see the same dynamics (or some of the dynamics) as are present in the bulk liquid, the analysis of the bulk is reduced to the consideration of only a few molecules. Furthermore, the presence or absence of specific bulklike dynamics in a sample of only a few molecules may be used to ascertain whether those dynamics are local or collective in nature. Two possible theoretical approaches, then, are (1) to analyze the dynamics of a small subset of a bulk simulation, and (2) to consider isolated clusters, and study their dynamics as a function of size and temperature. The former approach has been explored by Ohmine and co-workers.[12] We take the latter approach in this work. An advantage to considering clusters over simply looking at a small portion of a bulk simulation is that the cluster simulation may allow for a direct comparison with experiment.

[a]Present address: Department of Chemistry and Biochemistry, University of Texas at Austin, Austin, TX 78712.
[b]Present address: L-277, Chemistry and Materials Sciences Division, Lawrence Livermore National Laboratory, Livermore, CA 94450.

 0021-9606/93/064413-09$06.00

Water clusters are interesting in their own right, due, in part, to their presence in the earth's atmosphere.[15] These systems have been studied extensively by a variety of theoretical methods,[16–23] and the structures of the smaller clusters are well known. Cluster vibrations have been studied using MD,[16–18,21] and by using normal mode analysis based on Monte Carlo (MC),[20] molecular mechanics,[22] semiempirical,[21] and *ab initio*[21,23] determination of the structures. Plummer[21] has compared the vibrational frequencies of water pentamers, using MD (using a flexible model for the water, proposed by Stillinger and Rahman[24]), and using normal mode analysis based on structures generated by *ab initio* and semiempirical calculations. The three methods produced very different results. Additionally, the high frequency vibrations ($\omega > 1500\ \mathrm{cm}^{-1}$) of water clusters have been measured experimentally.[25,26] Recently, high-resolution IR studies of the dimer and trimer have been reported.[27]

In this work, we correlate the various intermolecular motions of the clusters with those of the bulk by comparing vibrational spectra as a function of cluster size. Such a comparison allows us to determine whether the observed modes are collective in nature, or whether they involve only a few molecules. We perform MD simulations, and calculate infrared absorption and Raman scattering spectra by Fourier transforming the autocorrelation functions of the dipole moment and polarizability, respectively. We present spectra for various sized clusters and for the bulk liquid, demonstrating that the liquid's dynamics may indeed be clarified by studying the clusters.

In addition, we explore here the effect of using an anisotropic polarizability for calculating the Raman and IR spectra of this system. Until now, most calculations of the IR and Raman signals of liquid water have used the nearly isotropic gas-phase polarizability tensor obtained by Murphy in 1977,[28] which was extracted from three gas-phase spectroscopic observables. In that work, the three polarizability components were obtained by measuring the depolarization ratio, optimizing a calculated rotational Raman spectrum to fit the experimentally obtained spectrum, and through the use of the best existing values of the frequency-dependent refractive index. The resulting polarizability tensor was found to be nearly isotropic, in contrast to most recent *ab initio* calculations.[29–31] In this work, we test two models for the polarizability tensor and demonstrate that a larger anisotropy is necessary to explain the presence of the librational peaks in the depolarized Raman signal of liquid water. This is also suggested by a comparison with recent femtosecond optical Kerr effect (OKE) measurements in liquid water.[32]

II. MODEL FOR INFRARED AND RAMAN LINE SHAPES

The Raman and IR spectra of a given sample may be calculated from the autocorrelation functions (ACFs) of the polarizability and dipole moment, respectively, of the sample; these are given by the sum of the individual molecular polarizabilities and dipole moments. Each molecule is characterized by a gas-phase (permanent) dipole moment $\boldsymbol{\mu}_{i,0}$ and polarizability tensor $\boldsymbol{\alpha}_{i,0}$. Interactions with neighboring molecules cause an induced dipole moment and polarizability on molecule i. We shall denote the values of the *in situ* dipole moment and polarizability of molecule i for a given configuration of molecules by $\boldsymbol{\mu}_i$ and $\boldsymbol{\alpha}_i$, respectively. We have employed the dipole–induced-dipole model, in which each molecule has a polarizable point dipole at its center of mass; the molecular dipole moment and polarizability are affected by those of the surrounding molecules by

$$\boldsymbol{\mu}_i = \boldsymbol{\mu}_{i,0} + \boldsymbol{\alpha}_{i,0} \sum_{j \neq i} \mathbf{T}_{ij} \boldsymbol{\mu}_j \tag{1}$$

and

$$\boldsymbol{\alpha}_i = \boldsymbol{\alpha}_{i,0} + \boldsymbol{\alpha}_{i,0} \sum_{j \neq i} \mathbf{T}_{ij} \boldsymbol{\alpha}_j . \tag{2}$$

Here $\mathbf{T}_{ij}$ is the dipole–dipole interaction tensor, given by

$$\mathbf{T}_{ij} = \frac{1}{|r_{ij}|^3} (3\hat{r}_{ij}\hat{r}_{ij} - \mathbf{1}). \tag{3}$$

In Eq. (3), $\hat{r}_{ij}$ is a unit vector in the direction $\mathbf{r}_i - \mathbf{r}_j$, where $\mathbf{r}_i$ and $\mathbf{r}_j$ are the positions of the centers of mass of molecules i and j, and $\mathbf{1}$ denotes a unit 3×3 tensor.

Calculations were performed for two different values of the gas-phase polarizability tensor: The (nearly isotropic) values of Murphy[28] ($\boldsymbol{\alpha}_{xx,yy,zz} = \{1.468, 1.528, 1.415\}$ Å^3, where the x axis is along the molecular dipole, and the molecule is in the xy plane), and a (more anisotropic) *ab initio* value ($\boldsymbol{\alpha}_{xx,yy,zz} = \{1.495, 1.626, 1.286\}$ Å^3), calculated by Huiszoon.[29] The latter value was chosen because the mean polarizability is virtually identical to the mean polarizability for the isotropic model, and because the anisotropy in Huiszoon's model for the polarizability gives approximately the correct intensity for the librational peak in the Raman spectrum of liquid water (see below). Previous, all MD calculations of the Raman spectrum of liquid water have employed the polarizability tensor obtained in Ref. 26,[9] or else simply assumed that the gas-phase polarizability is totally isotropic.[8]

In principle, Eqs. (1) and (2) can be solved for $\boldsymbol{\mu}_i$ and $\boldsymbol{\alpha}_i$ at a given configuration by matrix inversion; in practice, the first-order solution [i.e., the result from using $\boldsymbol{\mu}_{j,0}$ and $\boldsymbol{\alpha}_{j,0}$ in the far right of Eqs. (1) and (2)] was employed. A bulk simulation with $N = 100$ was performed which demonstrated that the polarizability obtained by matrix inversion did not give a noticeably different Raman signal from the first-order result.

Once the dipole moments of the water molecules have been calculated, the IR absorption signal is given by

$$\sigma(\omega) = \left(\frac{2}{\epsilon_0 c \hbar n}\right) \omega \tanh(\beta\hbar\omega/2)\,\mathrm{Re} \times \int_0^\infty dt\, e^{i\omega t} \langle \mathbf{M}(t) \cdot \mathbf{M}(0) \rangle, \tag{4}$$

where

$$\mathbf{M}(t) \equiv \sum_{j=1}^{N} [\boldsymbol{\mu}_j(t) - \langle \boldsymbol{\mu}_j \rangle] \tag{5}$$

is the sum of the individual molecular dipole vectors, and $\beta = 1/k_B T$ is the inverse temperature. n is the refractive index (which we take to be independent of frequency), ϵ_0 is the vacuum permittivity, and c is the speed of light.

In displaying the depolarized Raman spectrum, we use the ("reduced") representation $R(\omega)$, which contains a prefactor with a similar frequency and temperature dependence to the IR spectrum prefactor:[33]

$$R(\omega) = \frac{\omega}{(\omega_L - \omega)^4}(1 - e^{-\beta\hbar\omega}) \times \mathrm{Re}\int_0^\infty dt\, e^{i\omega t}\langle \Pi_{xz}(t)\Pi_{xz}(0)\rangle, \tag{6}$$

where

$$\Pi(t) \equiv \sum_{j=1}^{N} [\alpha_j(t) - \langle \alpha_j \rangle], \tag{7}$$

and ω_L is the frequency of the exciting laser. This form of the Raman spectrum is proportional to the sample response function (times the Raman frequency);[33] furthermore, it has the advantage of enhancing the higher-frequency contributions to the signal, and minimizing the contribution of the Rayleigh peak. An alternative to the $R(\omega)$ format is the Bose–Einstein corrected spectrum,[3,7] which is identical to Eq. (6), except that the ω prefactor is not included. These two forms are commonly used to display the low-frequency Raman spectrum. It should be noted that off-resonant nonlinear optical spectroscopies such as the optical Kerr effect and impulsive scattering may also be calculated from the polarizability ACF.[34]

III. SIMULATION PROCEDURE

Both the clusters and the bulk calculations were performed using the program MD++, developed in our group.[35,36] This program has previously been used to calculate the nonlinear optical response of a solute in water.[35] The (rigid) enhanced SPC/E model[37] for water, which accounts for water–water interactions via point charges on the atoms and oxygen–oxygen Lennard-Jones interactions, was employed. The molecular propagation was done using the "leapfrog" Verlet algorithm[38] for both the molecular centers of mass and the orientational variables (quaternions).

Cluster starting configurations were prepared by performing ~100 000 Monte Carlo (MC) cycles, during which the temperature was ramped from some high temperature to the desired temperature. Following this, ~20 000 MC cycles were performed at the desired temperature, as a means of ensuring equilibration. Then, ~50 000 MD steps were performed, to ensure equilibration of velocities, followed by the data-generating runs. During MD, the velocities were rescaled every 20 fs or so, to maintain the conservation of energy. The time step was chosen to be small enough so that the molecular velocities had to be changed by less than 1% (with only a few exceptions during the entire simulation). A time step of 1 fs was used for the larger clusters ($N=20$, 50), and a 0.5 fs time step was used for $N=5$ and 8. It was necessary to use a time step of 0.1 fs for the dimer. During the MC portions of the simulations, a confining sphere was placed around the cluster; this was not done during the MD portions. The clusters were thus free to dissociate during the MD portion of each run; however, this did not occur during any of the simulations reported here. The data-collecting runs were fairly long, with propagation times of 2.1 ns being used to generate most of the results. It should be noted that the spectra calculated in this work have been generated using a single (long) MD run; as such, the lower-temperature clusters may not have enough energy to isomerize, and thus may not represent the complete distribution of cluster geometries.

The bulk simulation consisted of 216 molecules in a cubic box with periodic boundary conditions.[38] The environment surrounding the box was treated as a dielectric continuum, and a reaction field (with $\epsilon=70$) was employed to account for long-range forces outside of the box.[38] The sample was brought near room temperature using 16 000 MC steps, and the data collection was performed over 524 ps. The average temperature during MD was 310 K. It was noted, for the case of the polarizability, that this very long simulation time was necessary in order to ensure that the sample appeared isotropic; that is, the autocorrelation functions for the three independent off-diagonal elements of the polarizability produced nearly identical contributions to the calculated Raman signal.

The sample polarizability and dipole moment were calculated every 8 fs during the bulk run and every 16 fs during the cluster runs. After the polarizability and dipole ACFs were calculated and averaged over the laboratory-frame axes, the ACFs were multiplied by a Gaussian decay term; hence, the long-time (and therefore unreliable) portions of the ACFs were neglected. This smoothing procedure is equivalent to imposing a Gaussian frequency resolution on the experiment; the cluster spectra were taken to have a 5 cm^{-1} resolution, and the bulk spectra were taken to have a 10 cm^{-1} resolution.

To calculate the classical ACFs from the time-dependent polarizability and dipole moment, we employed the Wiener–Khinchin theorem,[39] that is

$$C_{\mathrm{M,cl}}(\omega) \equiv \int_{-\infty}^{\infty} dt\, e^{i\omega t} C_{\mathrm{M,cl}}(t) = |\mathbf{M}(\omega)|^2, \tag{8}$$

where

$$C_{\mathrm{M,cl}}(t) \equiv \langle \mathbf{M}(t) \cdot \mathbf{M}(0) \rangle \tag{9}$$

and

$$\mathbf{M}(\omega) \equiv \int_0^\infty dt\, e^{i\omega t}\mathbf{M}(t). \tag{10}$$

(The above formulas, and the following reasoning, apply to Π as well as $\mathbf{M}$.)

Since the autocorrelation function has been calculated using a classical simulation, its Fourier transform is symmetric with respect to frequency; that is, it does not satisfy the detailed balance condition:

$$C_M(\omega) = \exp(\beta\hbar\omega) C_M(-\omega), \tag{11}$$

where $C_M(t)$ is defined analogously to Eq. (9). We may partially account for quantum effects in the spectrum by desymmetrizing $C_{M,cl}(\omega)$ so that the resulting function obeys Eq. (11). This is done by assuming some relation between the classical ACF and the quantum ACF. The detailed balance condition relates the Fourier transforms of the real and imaginary parts of the ACF to the full ACF spectrum by

$$C'_M(\omega) = \tfrac{1}{2}(1+e^{-\beta\hbar\omega}) C_M(\omega), \tag{12}$$

$$C''_M(\omega) = -\frac{i}{2}(1-e^{-\beta\hbar\omega}) C_M(\omega), \tag{13}$$

where $C'_M(\omega)$ and $C''_M(\omega)$ are the Fourier transforms of the real and imaginary parts, respectively, of the (quantum) ACF [defined analogously to Eq. (8)]. It should be noted that $C'_M(\omega)$ is an even function of frequency, while $C''_M(\omega)$ is an odd function of frequency. We may derive an expression for $C_M(\omega)$ by considering the high-temperature limit of Eq. (12); we obtain

$$C_M(\omega) = \frac{2}{1+e^{-\beta\hbar\omega}} C_{M,cl}(\omega). \tag{14}$$

A similar expression may be derived from the high-temperature limit of Eq. (13). Another procedure,[40] due to Egelstaff,[41] is derived from the high-temperature limits of both Eqs. (12) and (13); we have found that Egelstaff's procedure produces results which are qualitatively the same as produced by Eq. (14), so we shall use the simpler procedure, Eq. (14), in this work.

IV. RESULTS AND DISCUSSION

A. Raman spectrum of bulk water

Since the IR spectrum of liquid water has been very accurately calculated in Ref. 13, we shall focus on the Raman signal in this section. In Fig. 1, we compare our calculated Raman spectra, using both the nearly isotropic polarizability (IP) of Ref. 28 and the more anisotropic polarizability (AP) of Ref. 29, to experiment. In this figure (only) we use the Bose–Einstein expression for the signal, which brings out more clearly the 60 cm^{-1} peak. We have begun the plots at 25 cm^{-1}, in order to exclude the Rayleigh contribution to the spectra. The top frame gives the experimental result [reproduced from Fig. 1 of Ref. 3(c)], and the second and third frames are the AP and IP calculations, respectively. Noticeably absent in the IP result is the librational peak, which appears only as a long tail on the 170 cm^{-1} peak. This absence is consistent with previous simulations,[9] but not with experiment, where the librational motions produce a distinct peak in the spectrum. This dependence of the librational peak on the anisotropy of the polarizability makes sense when one considers that a libration is a hindered rotation which does not affect the polarizibility if it is isotropic.

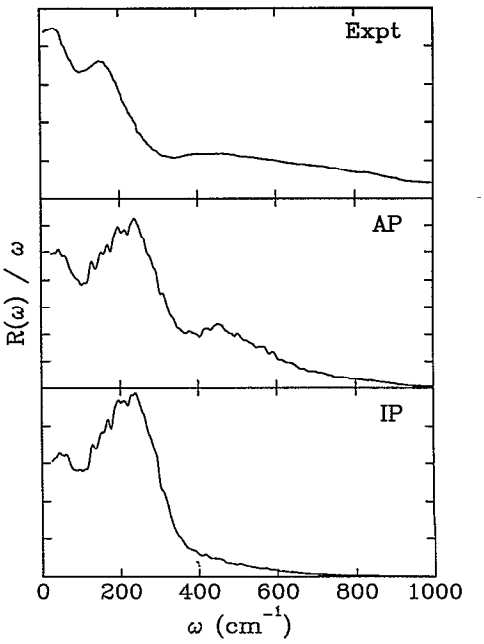

FIG. 1. The Bose–Einstein corrected Raman signal $[R(\omega)/\omega]$ of liquid water. Top: Experimental results, taken from Fig. 1 of Ref. 3(c). Center: Calculated (AP) results, using the calculated polarizability tensor from Ref. 27. Bottom: Calculated (IP) results, using the experimentally obtained polarizability tensor of Ref. 26.

Overall, the features of the experimental spectrum are reproduced fairly well by the AP simulation. In the calculated spectra, the 170 cm^{-1} peak actually appears at around 220 cm^{-1}. This is the approximate location of that peak in the Raman spectrum of ice, and may be different from the experimental result because of the tendency of MD simulations of liquid water to overemphasize the tetrahedral structure of the liquid.[42] Path integral Monte Carlo calculations[43] have shown that the inclusion of quantum effects reduces this discrepancy somewhat. The 60 cm^{-1} peak is too weak, relative to the 170 cm^{-1} peak, in both of the calculated results; the AP peak height is somewhat better than in the IP result. Additionally, the higher-frequency librational modes seem to be underrepresented in the AP simulation results. At such high frequencies, however, the classical simulation could be less accurate than at lower frequencies. Figure 1 gives direct evidence for the anisotropic nature of the gas-phase polarizability of water. The simulation suggests that the polarizability of water must be less isotropic than was determined in Ref. 28; otherwise, the librational modes would not be Raman active.

The presence of the 60 and 170 cm^{-1} peaks in the simulated Raman spectrum of water indicates that these features may be accounted for without the intramolecular structural changes associated with hydrogen bonding. This is not to say, however, that the hydrogen bonds do not play a role in the origin of these peaks. Although the simula-

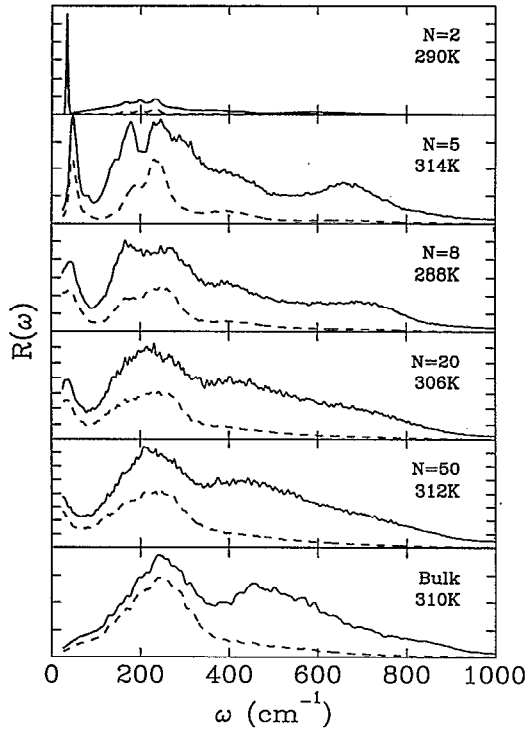

FIG. 2. Raman spectra for water clusters, as a function of size. The solid and dashed curves are the AP and IP results, respectively.

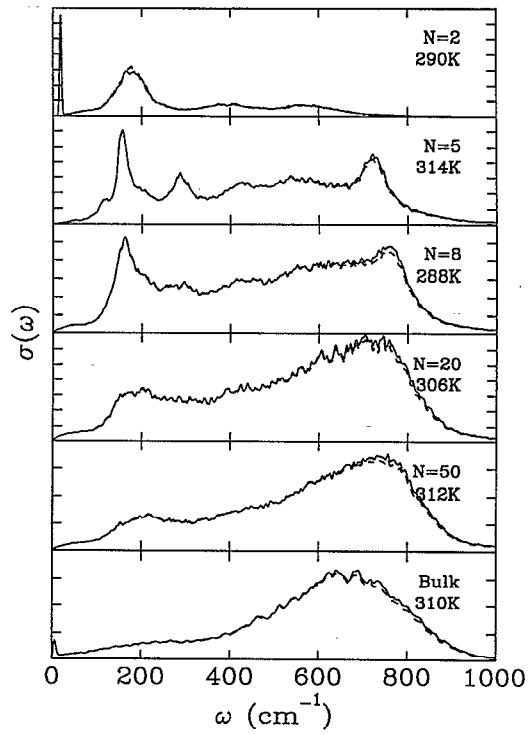

FIG. 3. IR spectra for water clusters, as a function of size. The solid and dashed curves are the AP and IP results, respectively.

tions do not include the hydrogen bonding in any explicit way, rigid-molecule simulations of water have been demonstrated to do a reasonable job of reproducing the structural and dynamical features of the liquid;[44] this indicates that the hydrogen bonds are being accounted for in some averaged way. The inclusion of intramolecular degrees of freedom could improve the agreement of both the relative peak heights in the 60 and 170 cm^{-1} peaks and the position of the latter peak.

B. Raman and infrared spectra of room-temperature clusters

Figure 2 gives the Raman [$R(\omega)$] spectra for a series of cluster sizes, as well as the bulk, for temperatures near room temperature. The solid curves were obtained from simulations using the anisotropic polarizability (AP) of Ref. 28; the dashed curves were obtained from the nearly isotropic polarizability (IP) of Ref. 29. As in Fig. 1, we have eliminated the Rayleigh peak by starting the plot at 25 cm^{-1}. It should be noted that the 60 cm^{-1} peak in the bulk liquid, which appears only as a faint shoulder in the bottom frame of Fig. 2, is clearly present in the Bose–Einstein representation of the same data (cf. Fig. 1).

Figure 2 demonstrates how the Raman signals of the clusters converge, as a function of size, to the bulk. The dimer (as one might expect) is the main exception to that series; in the dimer spectrum, the lowest- and highest-frequency peaks are redshifted relative to the $N=5$ spectrum, whereas the overall trend is a redshifting of these peaks with increasing size. The reason for this behavior is probably that the two molecules in the dimer have a larger range of rotational mobility. That the peak which appears at 45 cm^{-1} in the pentamer is of the same origin as the 60 cm^{-1} peak present in the bulk is somewhat doubtful, as it redshifts, as a function of size from 45 cm^{-1} in the $N=5$ spectrum to 25 cm^{-1} in the $N=50$ spectrum. As size is increased, we see that the peaks which are near 45 and 700 cm^{-1} in the pentamer diminish (or broaden), and shift to the red; the 700 cm^{-1} peak is not clearly resolved in the larger clusters. Additionally, the 200 cm^{-1} peak has a distinct bimodal structure in the smaller clusters; this suggests that there may be more than one type of motion contributing to that peak.

Overall, it is clear that the anisotropy of the gas-phase polarizability plays an important role in the Raman spectra of these systems. The peaks in the AP spectra are more intense than in the IP spectra, and the AP spectra show different ratios of peak heights. The latter effect may be used to establish which spectral features result from motions which are of a primarily rotational origin, and which are mainly hindered translations.

In Fig. 3, we present the IR spectra of the same cluster systems as in Fig. 2. As before, the solid curves are the AP results and the dashed curves are the IP results. Although the molecular polarizability does enter into the magnitude of the induced dipoles [cf. Eq. (1)], we see that the IR spectra are almost completely insensitive to the anisotropy of the polarizability. This can be explained by considering the importance of the gas-phase polarizability in the expressions for the Raman and IR spectra: In the Raman signal, the polarizability ACF is measured directly, whereas in the IR, the polarizability contributes only in the

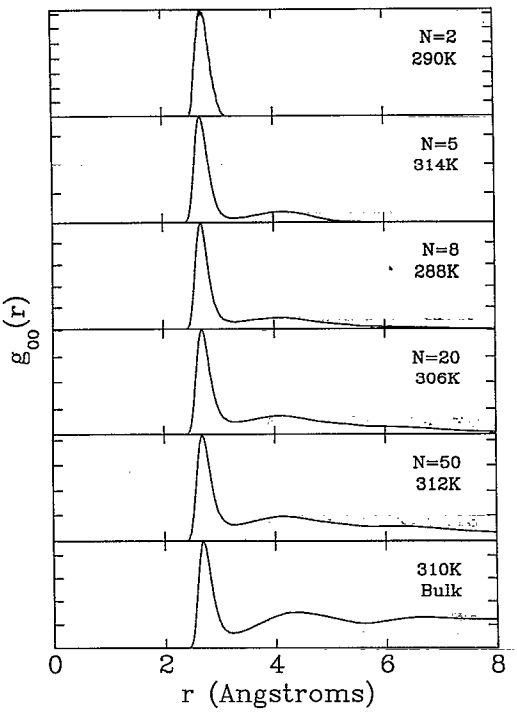

FIG. 4. Oxygen–oxygen radial distribution functions for the water cluster runs which generated Figs. 2 and 3.

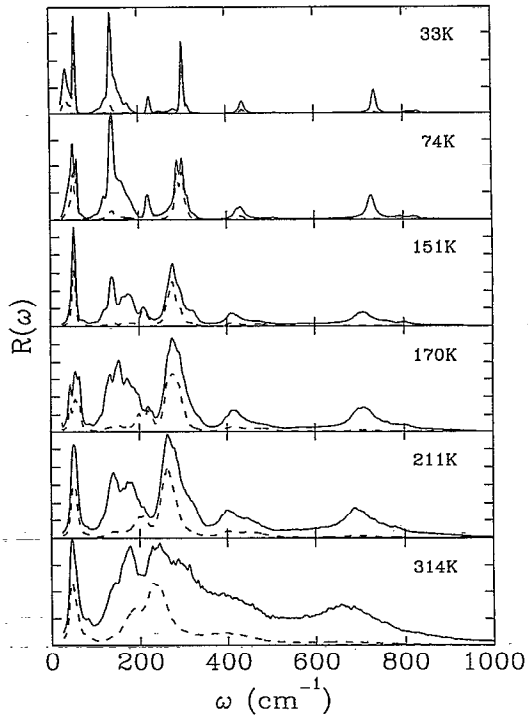

FIG. 5. Raman spectra for water pentamers, as a function of temperature. The solid and dashed curves are the AP and IP results, respectively.

correction to the spectrum arising from the permanent dipole moment. As with Fig. 2, we see that Fig. 3 displays a convergence to the bulk behavior as a function of cluster size, and again the highest-frequency peak in the dimer spectrum is redshifted relative to $N=5$. As a function of cluster size, we again see that the highest-frequency feature is redshifted. In the IR spectra, however, the 200 cm^{-1} peak gradually broadens with increasing cluster size, until it is only a shoulder in the bulk spectrum. An additional peak, at around 300 cm^{-1}, is clearly present in the pentamer, and quickly broadens as a function of cluster size. This feature is not distinguishable in either the dimer spectrum or the bulk spectrum.

Figure 4 gives the oxygen–oxygen radial distribution functions (RDFs) for the cluster runs used to generate Figs. 2 and 3. The fact that the peaks in $g_{OO}(r)$ are not well separated, indicates that the clusters do not have a rigid (solidlike) structure; otherwise, there would be zero in the RDF between the first two peaks.

C. Temperature dependence of pentamer spectra

In Fig. 5, we give the Raman spectra for a series of water pentamers, as a function of temperature. We see that the peak near 45 cm^{-1} has a distinct bimodal character at lower temperatures. This peak broadens only slightly as the temperature is increased, and shifts to the red just a few cm^{-1}. There is also a peak near 140 cm^{-1}, which broadens considerably as a function of temperature. A higher-frequency shoulder (at 150–170 cm^{-1}) grows in as a function of temperature, until it surpasses the 140 cm^{-1} peak in magnitude at room temperature. In the 33 K spectrum, there is a sharp peak at 300 cm^{-1}, which broadens considerably as the temperature increases. This peak, together with the 140 and 170 cm^{-1} peaks, make up the $\approx$200 cm^{-1} structure, which is seen in the bulk spectrum (cf. Fig. 2). Also of note is the rather sharp feature near 735 cm^{-1} in the 33 K spectrum, which is seen to broaden considerably, and to redshift by 75 cm^{-1} in the spectra displayed here. This peak is in the librational region of the spectrum, and comparison with the IP result shows that it is primarily rotational in nature.

Figure 6 gives the IR spectra corresponding to the same pentamer runs as in Fig. 4. In the top spectrum, we see that the principal features are near 160, 250, 500, and 820 cm^{-1}. These all broaden as the temperature is increased. Additionally, a small feature near 300 cm^{-1} is seen to grow in as a function of temperature; it is quite pronounced in the 314 K spectrum. The two higher-frequency peaks (at 500 and 820 cm^{-1}) are seen to undergo significant redshifts (70 and 100 cm^{-1}, respectively); this trend seems to be typical of the librational modes of water. The temperature-dependent redshifting of the librational peaks can be understood in that the molecules have more energy to move at higher temperatures, and thus have larger amplitude librational motions, with lower characteristic oscillation frequencies.

The geometries of the pentamers were examined by displaying representative portions of the simulations on a computer screen. It was observed that for all of the pentamer runs calculated here, the ring configuration, shown in Fig. 7, was preferred. This has been previously calculated to be the lowest energy structure.[16,19] In fact, no sig-

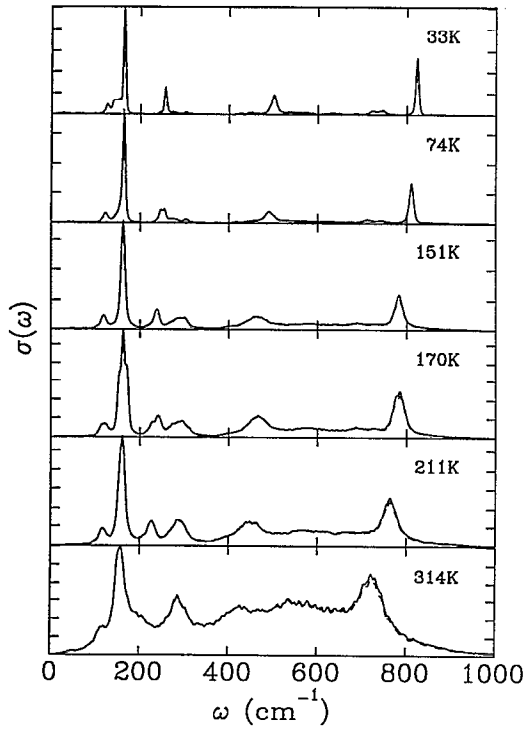

FIG. 6. IR spectra for water pentamers, as a function of temperature. The solid and dashed curves are the AP and IP results, respectively.

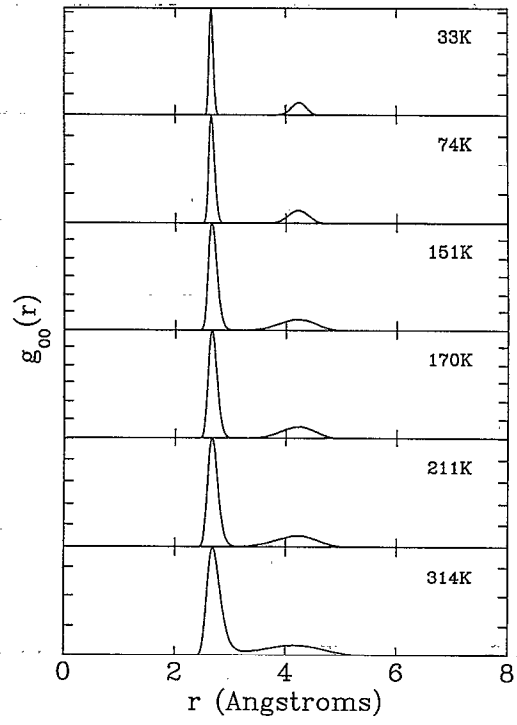

FIG. 8. Oxygen–oxygen radial distribution functions for the water pentamer simulations used to generate Figs. 5 and 6.

nificant isomerization (e.g., the interchanging of two water molecules or the adaptation of a structure radically different from the ring) occurred during the viewing of any but the highest temperature run. Clearly, then, it is not the case that all of the bulk's dynamics are present in the pentamer; however, it appears that virtually all of the liquid's modes in the frequency range 25–1000 cm^{-1} are also present in the pentamer. As the temperature was raised, more puckering of the ring occurred. This is in agreement with the results of Ref. 16, which found that water pentamers at lower temperatures lack the energy necessary to change from their initial configurations.

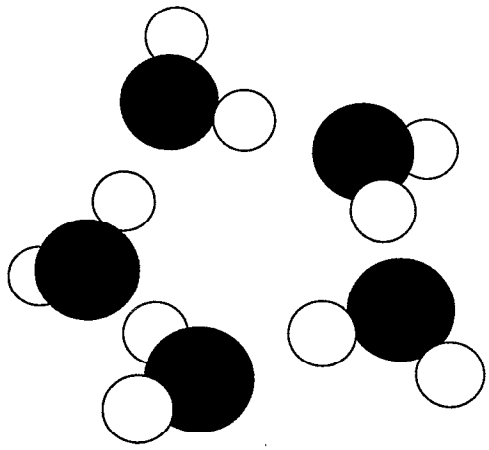

FIG. 7. The ring configuration for the water pentamer, which is preferred in all of the MD runs presented in this work.

The aforementioned qualitative observations are confirmed by Fig. 8, where we give the oxygen–oxygen radial distribution functions (RDFs) for representative samples (524 ps near the middles of the runs) of the pentamer simulations. In the top (33 K) frame, we see two relatively sharp peaks in the RDF, indicating that each oxygen has two neighboring oxygens at around 2.65 Å, and two neighbors at around 4.25 Å. This is clearly consistent with the observation that the pentamer is in an evenly spaced five-membered ring. As the temperature is raised to 170 K, there is little change in the structure—just some broadening of the peaks, indicating that the amplitudes of the intermolecular vibrations are getting somewhat larger. In the 314 K run, however, the two peaks in the RDF are connected, indicating that the cluster isomerizes somewhat. That the RDF is of the same basic shape as in the lower temperature indicates that the ring structure is still preferred; however, the cluster has sufficient energy to undergo some isomerization (the portion of the simulation viewed on the computer screen revealed a short time when the cluster formed a four-membered ring, with the fifth molecule connected to one of the vertices).

V. CONCLUSIONS

We have presented here the Raman and IR spectra for liquid water and a series of water clusters. The quantitative agreement found in the calculated IR spectrum of liquid water[13] demonstrates that MD simulations are capable of reproducing the librational motion found in the liquid. The lack of a librational peak in previous Raman simulations is therefore due to a deficiency in the model for the polariz-

ability, rather than some inherent problem with the classical MD simulation. The calculated Raman spectra in Fig. 1 demonstrate that the anisotropic polarizability of Ref. 29 produces a more realistic Raman spectrum than does the isotropic polarizability of Ref. 28. In the cluster spectra, we have found that there are some bulklike dynamics in even the smaller clusters. Although we have made no attempt here to isolate the specific nuclear motions underlying the observed spectral peaks, we have demonstrated that many of the motions in even the water pentamer (which, owing to its ringlike configuration, can certainly not be viewed as a realistic subset of a bulk liquid), are at the same frequencies which characterize the bulk dynamics. We have further shown that the librations in the pentamer become redshifted as the temperature of the cluster is increased.

In conclusion, we make the following two comments. Equation (6) is derived by assuming that the exciting laser is tuned far below any electronic transitions and far above the nuclear transition frequencies.[45] The contribution of the permanent dipole moment to the Raman signal is thus neglected. We have calculated this contribution by evaluating the Liouville space pathways which contribute to the nonlinear response function; we obtained[46]

$$R_{\mathrm{PD}}(\omega)=\frac{\omega}{(\omega_L-\omega)^4}(1-e^{-\beta\hbar\omega})\mathrm{Re}\frac{i\hbar\beta\omega}{\omega_L\omega_S}\times\int_0^\infty dt\, e^{i\omega t}\langle \mathbf{M}_x(0)\Pi_{xz}(t)\dot{\mathbf{M}}_z(0)\rangle, \quad (15)$$

where ω_L and ω_S are the laser and scattered frequencies, respectively. Equation (15) should be added to Eq. (6) to obtain the full Raman signal. We have performed a calculation to test the importance of Eq. (15) (assuming $\omega_L \approx \omega_S = 20\,000\ \mathrm{cm}^{-1}$), and found that its contribution to the Raman spectrum of liquid water is indeed negligible compared to that of Eq. (6). In the case of a molecule with a large permanent dipole and a relatively small polarizability or for a lower excitation frequency, however, the contribution of Eq. (15) to the Raman signal could well be important.

Examination of Eqs. (1) and (4) [or Eqs. (2) and (6)] raises the question of the relative magnitudes of the permanent dipoles (polarizabilities) and induced dipoles (polarizabilities) to the observed IR (Raman) signal (the so-called "allowed" and "interaction-induced" components). This question is indeed an intriguing one, but it is not answered here. Previous works[9,13] have calculated these two contributions separately, to provide such a comparison. This separation, however, does not account for the fact that the interaction-induced polarizability is built into empirical potential (in this case SPC/E) which governs the nuclear dynamics of the molecules.[37,44] We thus feel that the true distinction between "allowed" and "interaction-induced" contributions to the signal may only be truly made using a model for the water dynamics which explicitly includes the interaction-induced polarizability,[47] and comparing the results of simulations in which the dynamics have been performed with and without the influence of the molecular polarizability.

ACKNOWLEDGMENTS

We wish to thank Professor G. Fleming, Professor J. Muenter, and Professor G. Walrafen for useful discussions. The support of the National Science Foundation and the Air Force Office of Scientific Research is gratefully acknowledged.

[1] A. Rahman and F. H. Stillinger, J. Chem. Phys. **55**, 3336 (1971).
[2] O. F. Nielsen, Chem. Phys. Lett. **60**, 515 (1979).
[3] (a) G. E. Walrafen, M. R. Fisher, M. S. Hokmabadi, and W.-H. Yang, J. Chem. Phys. **85**, 6970 (1986); (b) G. E. Walrafen and M. R. Fisher, in *Biomembranes, A Volume of Methods of Enzymology*, edited by L. Packer (Academic, New York, 1986); (c) G. E. Walrafen, M. S. Hokmabadi, and W.-H. Yang, J. Chem. Phys. **88**, 4555 (1988).
[4] A. De Santis, R. Frattini, M. Sampoli, V. Mazzacurati, M. Nardone, M. A. Ricci, and G. Ruocco, Mol. Phys. **61**, 1199 (1987); P. Benassi, V. Mazzacurati, M. Nardone, M. A. Ricci, G. Ruocco, A. De Santis, R. Frattini, and M. Sampoli, *ibid.* **62**, 1467 (1987); P. Benassi, V. Mazzacurati, M. Nardone, M. A. Ricci, G. Ruocco, and G. Signorelli, J. Chem. Phys. **88**, 4553 (1988).
[5] M. H. Brooker, G. Hancock, B. C. Rice, and J. Shapter, J. Raman Spectrosc. **20**, 683 (1989).
[6] G. E. Walrafen, J. Phys. Chem. **94**, 2237 (1990).
[7] K. Mizoguchi, Y. Hori, and Y. Tominaga, J. Chem. Phys. **97**, 1961 (1992).
[8] P. A. Madden and R. W. Impey, Chem. Phys. Lett. **123**, 502 (1986); R. W. Impey, P. A. Madden, and I. R. McDonald, Mol. Phys. **46**, 513 (1982).
[9] (a) M. A. Ricci, G. Ruocco, and M. Sampoli, Mol. Phys. **67**, 19 (1989); (b) V. Mazzacurati, M. A. Ricci, G. Ruocco, and M. Sampoli, Chem. Phys. Lett. **159**, 383 (1989).
[10] O. Matsuoka, E. Clementi, and M. Yoshimine, J. Chem. Phys. **64**, 1351 (1976).
[11] W. L. Jorgensen, J. Chandrasekhar, J. M. Madura, R. W. Impey, and M. L. Klein, J. Chem. Phys. **79**, 926 (1983).
[12] I. Ohmine and M. Sasai, Prog. Theor. Phys. Suppl. **103**, 61 (1991), and references contained therein.
[13] B. Guillot, J. Chem. Phys. **95**, 1543 (1991).
[14] H. J. Berendsen, J. P. M. Postma, W. F. Van Gusteren, and J. Hermans, in *Intermolecular Forces*, edited by B. Pullman (Reidel, Dordrecht, 1981), p. 331.
[15] X. Yang and A. W. Castleman, J. Geophys. Res.-Atmosph. **96**, 2573 (1991).
[16] P. L. M. Plummer and T. S. Chen, J. Chem. Phys. **86**, 7149 (1987).
[17] P. L. M. Plummer and T. S. Chen, J. Phys. Chem. **87**, 4190 (1983).
[18] I. P. Buffey, W. B. Brown, and H. A. Gebbie, J. Chem. Soc. Faraday Trans. **86**, 2357 (1990).
[19] K. S. Kim, M. Dupuis, G. C. Lie, and E. Clementi, Chem. Phys. Lett. **131**, 451 (1986).
[20] J. R. Reimers and R. O. Watts, Chem. Phys. **85**, 83 (1984).
[21] P. L. M. Plummer, J. Mol. Struct. **237**, 47 (1990).
[22] C. E. Dykstra, J. Chem. Phys. **91**, 6472 (1989).
[23] E. Honegger and S. Leutwyler, J. Chem. Phys. **88**, 2582 (1988); R. Knochenmuss and S. Leutwyler, *ibid.* **96**, 5233 (1992).
[24] F. H. Stillinger and A. Rahman, J. Chem. Phys. **68**, 666 (1978).
[25] M. F. Vernon, D. J. Krajnovich, H. S. Kwok, J. M. Lisy, Y. R. Shen, and Y. T. Lee, J. Chem. Phys. **77**, 47 (1982); D. F. Coker, R. E. Miller, and R. O. Watts, *ibid.* **82**, 3554 (1985).
[26] S. Wuelfert, D. Herren, and S. Leutwyler, J. Chem. Phys. **86**, 3751 (1987).
[27] N. Pugliano and R. J. Saykally, Science **257**, 1937 (1992); N. Pugliano and R. J. Saykally, J. Chem. Phys. **96**, 1832 (1992).
[28] W. F. Murphy, J. Chem. Phys. **67**, 5877 (1977).
[29] C. Huiszoon, Mol. Phys. **58**, 865 (1986).
[30] P. Raeymaekers, H. P. Figeys, and P. Geerlings, Mol. Phys. **65**, 925 (1988).
[31] G. Maroulis, J. Chem. Phys. **94**, 1182 (1991).
[32] N. Scherer and G. Fleming (private communication); R. J. D. Miller and S. Palese (private communication).
[33] W. F. Murphy, M. H. Brooker, O. F. Nielsen, E. Praestgaard, and J. E. Bertie, J. Raman Spectrosc. **20**, 695 (1989).
[34] L. C. Geiger and B. M. Ladanyi, Chem. Phys. Lett. **159**, 413 (1989).

[35] L. E. Fried, N. Bernstein, and S. Mukamel, Phys. Rev. Lett. **68**, 1842 (1992).
[36] L. E. Fried and S. Mukamel, J. Chem. Phys. **96**, 116 (1992).
[37] H. J. C. Berendsen, J. R. Grigera, and T. P. Straatsma, J. Phys. Chem. **91**, 6269 (1987).
[38] M. P. Allen and D. J. Tildesley, *Computer Simulation of Liquids* (Clarenden, Oxford, 1987).
[39] N. G. Van Kampen, *Stochastic Processes in Physics and Chemistry* (North-Holland, New York, 1981).
[40] J. Borysow, M. Moraldi, and L. Frommhold, Mol. Phys. **56**, 913 (1985).
[41] P. Egelstaff, Adv. Phys. **11**, 203 (1962).
[42] G. E. Walrafen (private communication).
[43] R. A. Kuharski and P. J. Rossky, J. Chem. Phys. **82**, 5164 (1985).
[44] K. Watanabe and M. L. Klein, Chem. Phys. **131**, 157 (1989).
[45] R. W. Hellwarth, Prog. Quantum Electron. **5**, 1 (1977).
[46] W. Bosma, Ph.D. thesis, University of Rochester, 1992.
[47] See, for example, P. Ahlström, A. Wallqvst, S. Engström, and B. Jönsson, Mol. Phys. **68**, 563 (1989).